DOI: 10.1002/cbic.200800843

Shuttling Gold Nanoparticles into Tumoral Cells with an Amphipathic Proline-Rich Peptide

Sílvia Pujals,[a] Neus G. Bastús,[b] Eva Pereiro,[c] Carmen López-Iglesias,[d] Víctor F. Puntes,[b] Marcelo J. Kogan,[e] and Ernest Giralt*[a, f]

Cell-penetrating peptides (CPPs) are a potential tool for intracellular delivery of different kinds of cargoes. Because of their growing use in nanobiomedicine, both for diagnostics and for treatment, metal nanoparticles are an interesting cargo for CPPs. Here, gold nanoparticles (AuNps) and the amphipathic proline-rich peptide SAP have been used. Conjugation of the peptide onto the AuNps was achieved by addition of a cysteine to the SAP sequence for thiol chemisorption on gold, and the attachment was confirmed by visible spectroscopy, dynamic light scattering (DLS), ζ-potential (ZP), stability towards ionic strength (as high as 1 M NaCl), X-ray photoelectron spectroscopy (XPS) and high-resolution transmission electron microscopy (HR-TEM) coupled to electron energy loss spectroscopy (EELS). AuNp-C-SAP internalization in HeLa cells was observed by three different microscopy techniques—TEM, confocal laser scanning microscopy (CLSM) and transmission X-ray microscopy (TXM)—and all of them have confirmed the effective intracellular delivery of AuNps by SAP.

Introduction

A promising strategy for intracellular delivery that has been consolidated over the last decade is the use of peptides with the capacity to translocate across the cytoplasmic membrane, known as cell-penetrating peptides (CPPs).[1] The most common feature of CPPs is the presence of positively charged amino acids, especially arginines.[2] Moreover, the addition of hydrophobic moieties to the peptide sequence has been found to increase cellular uptake considerably.[3] For these reasons, CPPs are often endowed with these two properties through the introduction of an amphipathic sequence.[4]

CPPs have the capacity to transport distinct types of cargoes—ranging from low-molecular-weight drugs to liposomes, plasmids, antibodies and nanoparticles (Nps)—into the cell.[5] Nps are of particular interest for diagnostic purposes and treatment because of recent advances in nanobiomedicine.[6] They have recently been extensively used for drug and gene delivery,[7] tissue engineering,[8] hyperthermia cancer therapy,[9] targeted drug delivery and imaging,[10] and magnetic resonance imaging contrast enhancement,[11] among other applications. This wide range of uses has arisen from the recent developments in material physics and chemistry[12] that have allowed the optical, magnetic and electrical detection of diverse states of biological systems and living organisms with the aid of nanomaterials.

Here we examine the use of metal Nps that have two parts: a metal core and an outer organic/inorganic-stabilising layer. The core can be made out of a variety of materials and it determines the optical and electric properties of the Nps; thanks to these physical properties, the core can be used for targeting and remote excitation. The organic or inorganic molecules decorating the metal core surface are exposed at the surface and directly interact with the biological media. The shell is thus the determinant part for the reactivity and interfacial interactions of the ensemble.

When the metal nanoparticle is considered as an entity (core and shell), several other properties are found, such as the "enhanced permeability and retention" effect, which causes an increased rate of nanoparticle distribution in tumour tissue and inflamed sites as a result of the presence of leaky vessels in this tissues.[13] Other properties that can result when a biomolecule is bound to a metal nanoparticle include decreased degradation of the biomolecule on the nanoparticle surface and

[a] S. Pujals, Prof. E. Giralt
Institut de Recerca Biomèdica, Parc Científic de Barcelona
Baldiri Reixac 10, 08028 Barcelona (Spain)
Fax: (+34) 934937126
E-mail: ernest.giralt@irbbarcelona.org

[b] N. G. Bastús, Prof. V. F. Puntes
Institut Català de Nanotecnologia, Campus UAB
08193 Barcelona (Spain)

[c] Dr. E. Pereiro
ALBA Synchrotron Light Source, Campus UAB
08193 Barcelona (Spain)

[d] Dr. C. López-Iglesias
Unitat de Microscòpia Electrònica i Reconeixement Molecular in Situ
Serveis Científico-Tècnics, Universitat de Barcelona
08028 Barcelona (Spain)

[e] Prof. M. J. Kogan
Department of Pharmacological and Toxicological Chemistry
University of Chile
Centro para la Investigación Interdisciplinaria Avanzada
en Ciencia de los Materiales (CIMAT)
1007 Santiago de Chile (Chile)

[f] Prof. E. Giralt
Departament de Química Orgànica, Universitat de Barcelona
Martí I Franqués 1, 08028 Barcelona (Spain)

Supporting information for this article is available on the WWW under http://dx.doi.org/10.1002/cbic.200800843.

 © 2009 Wiley-VCH Verlag GmbH & Co. KGaA, Weinheim

reduced renal clearance (the cut-off for renal clearance is around 5 nm), which causes increased half-lives of drugs and more prolonged pharmacological effects when conjugated to Nps.[14]

Due to the growing interest in the use of metal Nps in living systems, detailed cellular studies are required before their application in vivo for treatment or diagnosis purposes. Although Nps are generally used extracellularly, their intracellular use is of great interest as most of the important drug targets are located inside the cell. There have been some precedents in this area,[15] but research effort is still required in this field, because gaining access to the intracellular region should widen the use of Nps and consequently expand their therapeutic applications.

The cell-penetrating peptide Tat has already been used to achieve nanoparticle access to the intracellular region.[5,15] However, although it aids in transporting Nps into the cell nucleus, cell viability is compromised. Here we have used amphipathic Pro-rich peptides[16] derived from the N-terminal γ-zein, a maize storage protein. These represent one of the newest classes of CPPs, as a result of their demonstrated efficiency in translocation across the cytoplasmic membrane without presenting toxicity, both in cell cultures and in vivo.[17] The presence of a 50% proline content in the sequence ensures that the peptide adopts the three residues per turn periodicity of the polyproline II structure. An amphipathic helix can then be formed by placing hydrophobic amino acids at *i*/(*i*+2), (*i*+6)/(*i*+8), etc. and hydrophilic ones at (*i*+1), (*i*+7), etc. Of the peptides initially tested, $(VRLPPP)_3$, also known as sweet arrow peptide (SAP), was the most effective in cellular translocation. Furthermore, this peptide is not cytotoxic at concentrations up to 1 mM.[18]

As the metal nanoparticle component, gold Nps (AuNps) were chosen as SAP cargo because of their established non-cytotoxicity, stability, ease of preparation and controllable surface chemistry.[19] In addition, their excellent photonic properties offer several advantages for imaging: strong light scattering, brightness much higher than that of organic fluorophores, non-susceptibility to photobleaching, and ease of detection in the nM range.

AuNps have also been widely studied for biological purposes.[20] Their nanometric scale, together with their highly electron-dense and strongly metallic character, make them suitable for use as energy antennas for the local and remote manipulation of DNA[21] or protein aggregates,[22] and for medical hyperthermia,[23] as new vehicles for drug delivery,[24] or as scaffolds for antigen delivery.[25]

For all the aforementioned reasons, here we have tracked the cellular uptake of AuNps decorated with SAP by several microscopy techniques.

Results and Discussion

C-SAP conjugation to AuNps and characterisation

To attach SAP to AuNps the peptide with an N-terminal cysteine—C-SAP, or C-$(VRLPPP)_3$—was prepared by standard Fmoc/*t*Bu solid-phase peptide synthesis. This approach allowed the highly favourable thiol chemisorption on gold. The energetics of thiol–gold bond formation are complex, and several accounts relating to the nature and the geometry of binding and the diverse energetic pathways (through thiol radical, thiol or thiolate) that might be followed in order to form the bond have been reported. In the case of alkanethiols forming self-assembled monolayers, the consensus is that hydrogen atoms, from S–H, are generally dissociated during chemisorption.[26] In self-assembled monolayers, monolayer formation is also promoted by van der Waals interactions, which pack alkyl chains, thereby assisting conjugation. In the conjugation of peptides to an Au surface, a similar effect may occur because of electrostatic or hydrophobic interactions. In the case of peptides with amphipathic character, both kinds of interaction may help to pack several peptide copies on the Au surface. This feature could be an advantage when dealing with peptides presenting secondary amphipathicity: that is, peptides presenting hydrophilicity on one face of the helix and hydrophobicity on the opposite face, as is the case of SAP.

AuNps of 12 ± 1 nm in diameter were routinely synthesised by the well-established Turkevich method, in which a gold salt is reduced in aqueous sodium citrate solution, thereby producing nearly monodisperse spherical Nps over a tuneable range of sizes depending on the gold/citrate ratio.[27] C-SAP was rapidly coupled to these particles, in less than 15 min in aqueous solution at room temperature. The conjugation mechanism could be driven by an initial electrostatic interaction: that is, the positive amino N-terminal group in the vicinity of the thiol might significantly accelerate the thiol approach onto the gold nanoparticle surface.[28] Moreover, this interaction may be cumulative with that of the N-terminal primary amine, because amino groups are also known to display strong interaction with Au surfaces.[29] The conjugation was performed in the presence of excess peptide with rapid stirring to ensure full coverage of AuNps and a homogeneous process. The excess of peptide was later removed by dialysis.

Peptide-decorated AuNps were studied by visible spectroscopy, dynamic light scattering (DLS), ζ-potential (ZP), X-ray photoelectron spectroscopy (XPS) and high-resolution transmission electron microscopy (HR-TEM) coupled to electron energy loss spectroscopy (EELS). Visible spectroscopy showed that citrate-stabilised AuNps displayed a characteristic absorbance band at 519 nm. Once the C-SAP had been conjugated on the particle surfaces, we observed a red shift of about 12–14 nm in the surface plasmon resonance (SPR) band (see Figure 1A and C) caused by environmental changes in the dielectric constant around the surfaces of these particles.[30] The increase in the hydrodynamic size—about 8–12.3 nm for AuNps and 20.5 nm for AuNp-C-SAP—as shown by DLS further corroborated that peptide conjugation had taken place.

Moreover, C-SAP conjugation to AuNps was confirmed by the change in the surface charge by ZP measurements, from −38.2 mV for AuNps, because of the adsorbed citrate, to +6.6 mV in AuNp-C-SAP, because C-SAP possesses a +3 net charge at neutral pH as a result of its Arg residues. In addition, this change in the surface charge allowed us to discern the

 © 2009 Wiley-VCH Verlag GmbH & Co. KGaA, Weinheim

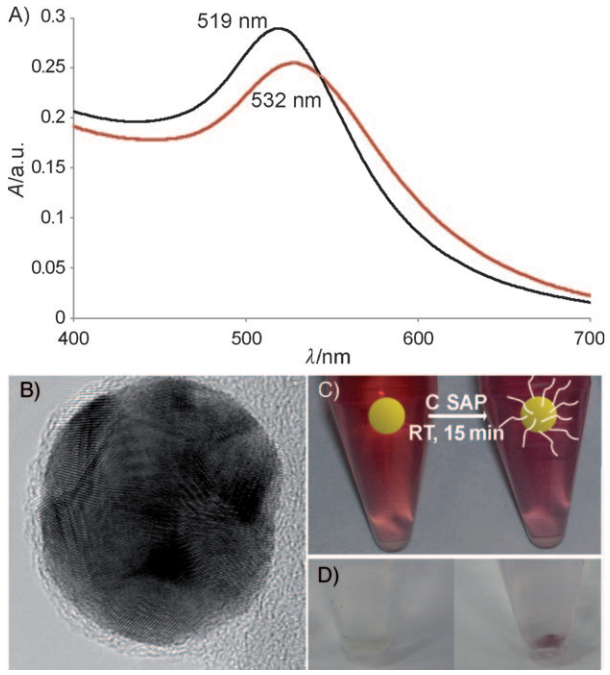

Figure 1. A) Visible spectra of AuNp (in black) and AuNp-C-SAP (in red) solutions. B) HR-TEM image of AuNp-C-SAP (×500 000). C) The absorption red shift in the conjugation process can be seen by the naked eye. D) Pellet of HeLa cells incubated with AuNp (left) or with AuNp-C-SAP (right).

nature of the nanoparticle stabilisation mechanism: from electrostatic in citrate-stabilised AuNps to steric/electrosteric stabilisation in AuNp-C-SAP.

This finding was further corroborated by study of the stability towards ionic strength, which also provided strong evidence of SAP attachment to the gold nanoparticle surface. The addition of increasing concentrations of sodium chloride caused citrate-stabilised AuNps to aggregate, the colour of the solution turned blue, and there was a clear shift in the plasmon band. This observation can be explained in terms of screening of the negative charge particle repulsion, which causes a decrease in interparticle distance,[31] ultimately leading to dipole coupling between the plasmons of neighbouring particles to form the aggregates.[30,32] When the peptide is attached to the Nps, high ionic strength does not affect its stability, because the AuNps are not in a colloidal state as a result of charge repulsion but as one of steric stabilisation (see Figure S1 in the Supporting Information).[33] An AuNp-C-SAP colloidal solution containing NaCl (1 M) remained stable for more than a month.

XPS was used to prove the presence of Au–S bonds on the AuNp surface.[34] In the case of peptide-conjugated AuNps, peaks from S2p, S2s and Au4f core levels were detected. The S2p signal consisted of a broad band with a maximum at 168 eV, which corresponded to the chemisorption of S onto Au. S2p and S2s core level peaks were not observed for citrate-stabilised AuNp (Figures S2 and S3 in the Supporting Information).

HR-TEM images of AuNp-C-SAP showed low electron density around the Nps, possibly reflecting the attachment of the peptide at their surfaces (see Figure 1 B, in contrast with AuNps, Figure S4 in the Supporting Information). Coupling HR-TEM to EELS confirmed, by identification of peaks at 288 and 296 eV and by sulphur mapping, that the low electron density corresponded to a thiol-containing molecule.

Cellular uptake of AuNp-C-SAP

To check whether and how C-SAP transported AuNps into the cell, HeLa cells were incubated with an AuNp-C-SAP solution for 3 h. They were then fixed, dehydrated and embedded in epoxy resin for TEM observation. In the centrifugation step immediately after fixation, the pellet of cells incubated with AuNp-C-SAP had a burgundy colour, possibly indicating the presence of AuNp-C-SAP. This visibly contrasted with the pellet from cells treated with AuNp, which was white (see Figure 1 D). After sectioning with an ultramicrotome and staining, we observed HeLa subcellular structures with ease and the nucleus was well defined. For cells treated with AuNp-C-SAP, AuNps were clearly visible as higher-contrast regions inside endosomes or attached to the cell membrane, possibly waiting to be taken up (see Figure 2, right-hand image). In contrast, the cells that had been incubated with citrate-stabilised AuNps revealed no uptake after exhaustive TEM observation (see Figure 2, left-hand image).

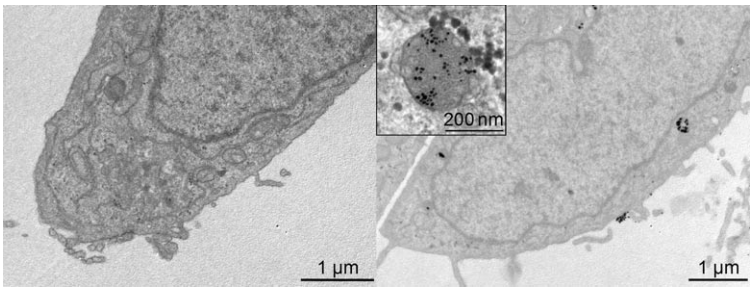

Figure 2. Electron micrographs of HeLa cells incubated with AuNps (left) or AuNp-C-SAP (right) for 3 h. The insert shows a magnification of an endosome full of AuNp-C-SAP.

At longer incubation times (4–5 h), the morphology of the vesicles containing the Nps changed significantly. The vesicles at later incubation times presented multimembrane structures with higher contrast: that is, they contained a higher proportion of organic material and probably corresponded to complex intracellular organelles containing smaller vesicles known as multivesicular bodies (see Figure 3). Multivesicular bodies are ultimately delivered to lysosomes, but they can also fuse back with late endosomes.[35]

After confirmation of AuNp-C-SAP uptake by TEM, confocal laser scanning microscopy (CLSM) was used to assess the uptake in living cells. CLSM is normally used to track fluorescently labelled molecules, but here the AuNps were visualised by the light they reflected when irradiated with a laser (confocal reflectance microscopy).[23,36] While the control cells and the

 © 2009 Wiley-VCH Verlag GmbH & Co. KGaA, Weinheim

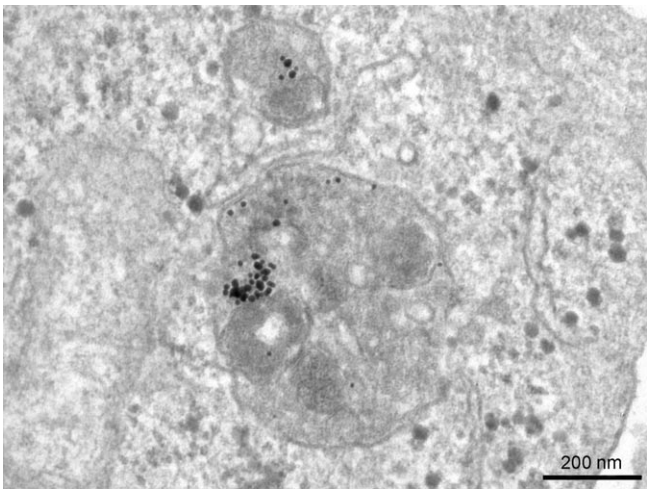

Figure 3. Electron micrograph of a HeLa cell incubated with AuNp-C-SAP for 5 h.

cells incubated with AuNps presented low reflection signals, those incubated with AuNp-C-SAP showed increased reflected light (Figure 4). In contrast to TEM, in which the ultrathin sections corresponded to a thickness of 50 nm, in CLSM the whole cell was viewed. Thus, after optical sectioning and spatial reconstruction of cells, CLSM allowed us to observe AuNp-C-SAP homogenously distributed throughout the cytoplasm. In all the experiments, contrast phase and bright field were used to assess normal cell morphology, and labelling of the cell membrane with Oregon green-wheat germ agglutinin confirmed that most of the reflection signal came from the intracellular region (see Figure S5 in the Supporting Information).

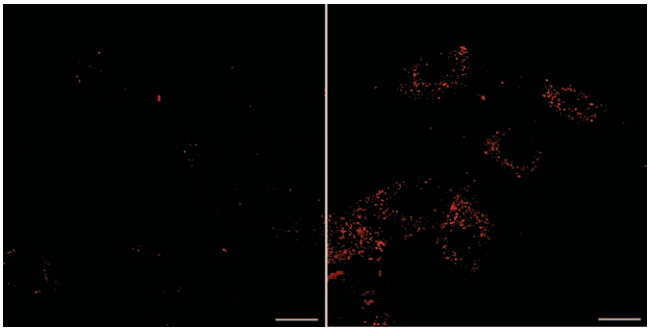

Figure 4. CLSM images of HeLa cells incubated with AuNps (left) or AuNp-C-SAP (right). Scale bar = 20 μm.

An emerging technique for imaging cells is transmission X-ray microscopy (TXM). Because X-rays have shorter wavelengths (0.3 nm to 5 nm) than visible light, higher spatial resolution can be achieved than with CLSM. In the case of sensitive samples the ultimate resolution is limited by radiation dose (up to about 10 nm),[37] but TXM can offer several advantages. It can produce images of relatively thick samples (up to 10 μm). Two-dimensional images with 15 nm resolution have been achieved recently, as well as tomographies of 50 nm. In particular, soft X-rays are used in the so-called water window range (284–543 eV), because cell structures can be visualised with good absorption contrast without staining as water is relatively transparent.[38]

Therefore, we visualised AuNp-C-SAP uptake by TXM at the BESSY synchrotron.[39] Many parameters still have to be optimised (the carbon film on the grid holding the samples, for example, interfered in the measurement because it prevented differential contrast between cell structures). However, the contours of HeLa cells and some darker spots, corresponding to AuNps groups, could clearly seen, because Au is more absorbing than C at the working energy of 520 eV (see Figure 5). As this was a preliminary attempt, the observation was performed on 500 nm thick sections of cryofixed cells. However, these sections are already one order of magnitude thicker than those used for TEM. To the best of our knowledge, this is the first report of observation of an internalisation event by TXM.

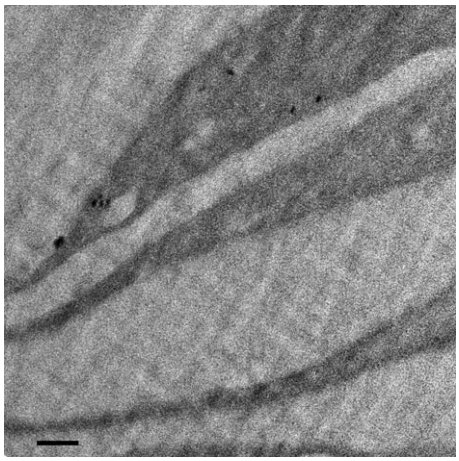

Figure 5. TXM image of HeLa cells incubated with AuNp-C-SAP. Scale bar = 1 μm.

Although toxicity is a crucial issue when dealing with Nps,[40] a detailed cytotoxicity study was out of the scope of this study. Checking the toxicity of Nps is complex because many parameters are involved. Not only are the core composition and size of the nanoparticle important, but the molecules decorating its surface, the sample concentration and the incubation time, as well as the cell line used also play a role. Although Au is an inert metal that should not cause toxicity, when it is surfacted with a toxic molecule such as cetyl trimethylammonium bromide it does have a toxic effect.[40a] As SAP does not show a cytotoxic effects up to concentrations of 1 mM,[18] we propose that its conjugation onto Au should not change its non-cytotoxic character. No significant difference in cell viability was observed between the control cells and those treated with citrate-stabilised AuNp or AuNp-C-SAP, as ascertained by the percentage of cells unstained with propidium iodide—a standard marker for dead cells—by flow cytometry after 24 h treatment at the highest concentration used for uptake studies (0.3 nM; see Figure S6 in the Supporting Information).

 © 2009 Wiley-VCH Verlag GmbH & Co. KGaA, Weinheim

Conclusions

In this study we have demonstrated that AuNps can be taken up by the cell through their conjugation to SAP. This finding has been confirmed by three microscopy techniques: TEM, CLSM and TXM.

The microscopy methods used in this study are complementary, because each presents several unique properties. The optimal resolution of TEM allows the detailed visualisation of subcellular structures involved in the internalisation process at a series of time points. CLSM allows the observation of living cells, thus providing a real-time study of the process. Moreover, sample preparation is straightforward, convenient and not time-consuming. Also, a further advantage not exploited in this study is the potential to combine reflection with fluorescence, and thus simultaneously follow metal Nps and fluorescently labelled molecules. With regard to TXM, the main advantages are that it allows work with thicker samples than TEM and visualisation of cellular structures without staining.

The excellent photonic properties of AuNps allow cellular uptake to be tracked by a wide range of techniques and thus provide detailed insight into the process; this is required in order to evaluate the interaction of these new nanoparticulate entities with cells.

It is difficult to find molecules that combine all the desired properties for a drug: high activity, capacity to home on its target and delivery to its therapeutic place of action. Nps may provide convenient scaffolds for unifying these properties by multiconjugation. The attachment to the nanoparticle of a vector—such as SAP—to allow access to the intracellular region, together with the drug itself and molecules for homing onto the desired target should result in a final entity with all the desired properties.

Experimental Section

Materials: Fmoc-Nα-protected amino acids were obtained from IRIS Biotech GmbH (Marktredwitz, Germany). The 2-chlorotrityl chloride resin was purchased from CBL-PATRAS (Patras, Greece). Coupling reagents: 7-azabenzotriazol-1-yloxytris(pyrrolidino)phosphonium hexafluorophosphate (PyAOP) was obtained from Applied Biosystems, benzotriazol-1-yloxytris(pyrrolidino)phosphonium hexafluorophosphate (PyBOP) from Novabiochem (Laüfelfingen, Switzerland), 1-hydroxy-7-azabenzotriazole (HOAt) from GL Biochem (Shanghai, China), and 2-(1*H*-benzotriazol-1-yl)-1,1,3,3-tetramethyluronium tetrafluoroborate (TBTU) from Albatross Chem Inc. (Montreal, Canada). Trifluoroacetic acid (TFA) was purchased from Scharlab S.L. (Barcelona, Spain). Piperidine, dimethylformamide (DMF), dichloromethane (DCM) and acetonitrile were from SDS (Peypin, France). *N*,*N*-Diisopropylethylamine (DIEA) was obtained from Merck (Darmstadt, Germany). Triisopropylsilane (TIS) was from Fluka. Hydrogen tetrachloroaurate(III) hydrate was purchased from Sigma.

Synthesis and chromatography: Peptides were synthesised by solid-phase synthesis by the 9-fluorenylmethoxycarbonyl/*tert*-butyl (Fmoc/*t*Bu) strategy. 2-Chlorotrityl resin, Nα-Fmoc-protected amino acids (2 equiv)/TBTU(2 equiv) and DIEA(6 equiv) were used. 2,2,4,6,7-Pentamethyldihydrobenzofuran-5-sulfonyl (Pbf) was used as a protecting group for the Arg side chain. The Fmoc protecting group was cleaved by treatment with a solution of piperidine in DMF (20%, 2×10 min). For incorporation of Fmoc-Arg(Pbf)-OH onto the growing peptide resin, TBTU was replaced with the more potent phosphonium salt PyBOP (2 equiv), which was pre-activated for 10 min before addition of the amino acid to the peptide resin. Peptides were cleaved from the resin by treatment with TFA (95%), TIS (2.5%) and water (2.5%) for 1 h 30 min and identified at $\lambda = 443$ nm by analytical RP-HPLC [Waters 996 photodiode array detector fitted with a Waters 2695 separation module, a Symmetry column (C_{18}, 5 μm, 4.6×150 mm) and the Millennium software; flow = 1 mL min^{-1}; gradient = 5–100% B over 15 min; A = TFA in H_2O (0.045%), B = TFA in acetonitrile (0.036%)]. Peptides were purified by semipreparative RP-HPLC [Waters 2487 Dual λ Absorbance Detector fitted with a Waters 2700 Sample Manager, a Waters 600 Controller, a Waters Fraction Collector, a Symmetry® column (C_{18}, 5 μm, 30×100 mm) and Millennium chromatography manager software]. HPLC conditions: flow = 10 mL min^{-1}. Gradient = 5–20% D over 5 min; 20–70% D over 30 min; 70–100% D over 5 min; C = TFA in H_2O (0.1%), D = TFA in acetonitrile (0.05%). Peptides were characterised by MALDI-TOF mass spectrometry (Voyager-DE RP MALDI-TOF, PE Biosystems with a 337 nm N_2 laser).

AuNp synthesis: AuNps were synthesised by the classical Turkevich[27] method. A sodium citrate solution (106 mL, 2.2 mM) was boiled for 10 min and $HAuCl_4$ (1 mL, 24.3 mM) was added with rapid stirring. After the solution colour had changed to red, it was further boiled for 15 min.

C-SAP conjugation to AuNps: C-SAP (20 μM) was added to a AuNp solution (1.5 nM) in sodium citrate (2.2 mM), and allowed to react with rapid stirring for 15 min at room temperature (RT). Dialysis (M.W.C.O. 6–8000) over sodium citrate (1 mM) was performed to remove excess peptide.

AuNp-C-SAP characterisation: Visible spectra were acquired with a Shimadzu UV-2400 spectrophotometer. For experiments on the stability with regard to ionic strength, an aqueous sodium chloride solution was added to AuNp or AuNp-C-SAP at increasing concentrations and visible spectra were acquired at each salt concentration. Dynamic light scattering (DLS) and ZP measurements were made with a Malvern ZetaSizer Nano ZS instrument operating at a light source wavelength of 532 nm and a fixed scattering angle of 173°. These measurements were carried out at pH 7.0; DLS size distribution was analysed by volume and ZP distribution by intensity. For XPS, AuNp or AuNp-C-SAP solution (10 μL) was placed on a silicon nitride surface and analysed with PHI ESCA-5500 equipment. A monochromatic $Al_{K\alpha}$ X-ray source was used and the chamber was maintained below 2×10^{-9} Torr. Spectra were analysed with the aid of Multipak software.

HR-TEM coupled to EELS with AuNp-C-SAP: Three drops (3× 20 μL) of AuNp-C-SAP solution were placed on a hollow Cu grid and allowed to dry at RT. All electron micrographs were obtained with a Jeol JEM 2010F electron microscope (Japan) operating at 200 KV coupled to an electron energy loss spectrometer.

Cell culture and incubation with AuNp-C-SAP: HeLa cells were obtained from ATCC (Manasas, VA) and cultured in DMEM (1000 mg per L-glucose, Biological Industries) containing foetal calf serum (FCS, 10%), glutamine (2 mM), penicillin (50 U mL^{-1}) and streptomycin (0.05 g mL^{-1}). Exponentially growing HeLa cells were detached from the culture flasks by treatment with a trypsin/EDTA (0.25%) solution, and the cell suspension was seeded at a concentration of 21.4×10^3 cells per cm^2 onto glass cover slips, 4-well Lab-Teck chambered coverglass, or plastic dishes (Nalge Nunc International, Rochester, NY), depending on the experiment. Experiments

 © 2009 Wiley-VCH Verlag GmbH & Co. KGaA, Weinheim

were carried out 24 h later, at approximately 60 to 70% confluence. AuNp or AuNp-C-SAP solutions were sterilised by 30 min exposure to UV light. Nonadherent cells were washed away, and attached cells were incubated in DMEM medium at 37 °C under CO_2 (5%) with a known concentration of AuNp or AuNp-C-SAP.

TEM of ultrathin sections of HeLa cells: HeLa cells were incubated with an AuNp or AuNp-C-SAP solution (0.3 nM) for 3 h, washed three times with PBS and fixed with glutaraldehyde (2.5%) for 1 h. Cells were detached from the Petri dish by scraping and centrifuged (4 °C, 2500 rpm, 10 min), thereby affording a compact pellet. After four 10 min washings with PB (0.1 M), cells were stained with OsO_4 (1%) for 1 h and washed again with PB (0.1 M, 10 min each wash). Cells were dehydrated at 4 °C through a series of acetone concentrations (50, 70, 90, 96, 100%), prior to being embedded in Spurr's epoxy resin. After cell embedment (60 °C, 48 h), sections with a thickness of 50 nm were cut with an ultramicrotome and placed on carbon-coated Cu grids. Finally, these grids were further enhanced with uranyl acetate. All electron micrographs were obtained with a Jeol JEM 1010 MT electron microscope (Japan) operating at 80 kV. Images were obtained on a Megaview III (ISIS, Münster, Germany).

CLSM: HeLa cells were incubated with an AuNp or AuNp-C-SAP solution (0.2 nM) for 2 h and were then washed three times with DMEM/FCS (10%) without phenol red. Oregon Green-WGA (1 μL) was then added and CLSM was performed with a Leica SPII microscope in the reflectance mode with a 63× objective and 488 nm excitation with an argon laser, thereby providing 0.25 μm-thick optical sections.

Transmission X-ray microscopy (TXM): HeLa cells were incubated with an AuNp or AuNp-C-SAP solution (0.2 nM) for 3 h, washed three times with PBS and fixed with glutaraldehyde (2.5%) for 1 h. After scraping, cryo-ultramicrotomy was performed, providing 500 nm-thick sections, which were placed onto carbon-coated Cu grids. Samples were then observed in a TXM at a synchrotron facility. Two-dimensional projections of the sample were recorded by absorption contrast imaging with a CCD camera with exposure times of around 1 s. The working energy was 520 eV, between the inner-shell absorption edges of carbon (284 eV) and oxygen (543 eV); that is, the water window range.[38]

Flow cytometry: For each assay, 21.4×10^3 cells per cm^2 were seeded and cultured for 24 h on plastic dishes. The culture medium was then discarded, and the cells were incubated for 3 h at 37 °C under CO_2 (5%) with fresh medium containing AuNp-C-SAP or AuNp as a negative control (0.3 nM). Cells were washed in PBS, treated with trypsin for 5 min at 37 °C and collected in plastic tubes in cold medium. After centrifugation (1000 rpm, 4 °C, 4 min), the trypsin-containing solution was discarded and the cells were resuspended in Hepes-buffered (25 mM) cell culture medium containing propidium iodide (5 $\mu g\,mL^{-1}$). Fluorescence analysis was performed with a Coulter XL flow cytometer. At least 10000 events per sample were analysed twice. The results shown are each the average of two measurements in the flow cytometer, and bars indicate the standard deviation.

Acknowledgements

This work was supported by MCI-FEDER (Bio2008-00799 NAN2004-09159-C04-02 and NANOBIOMED-CONSOLIDER) and the Generalitat de Catalunya (CeRBa and 2005SGR-00663). S. Pujals is supported by a FPU grant from the Ministerio de Ciencia e Innovación of Spain. The authors thank Dr. Raquel García Olivas and Dr. Jordi Arbiol for technical advice on CLSM and HR-TEM/EELS (UB-SCT), respectively, and P. Guttmann and J. Thieme for the TXM measurements performed at BESSY synchrotron.

Keywords: cell-penetrating peptides · drug delivery · gold nanoparticles · nanostructures · proline

[1] U. Langel, *Handbook of Cell-Penetrating Peptides*, CRC, Boca Raton, **2006**.
[2] a) D. J. Mitchell, D. T. Kim, L. Steinman, C. G. Fathman, J. B. Rothbard, *J. Pept. Res.* **2000**, *56*, 318–325; b) S. Futaki, T. Suzuki, W. Ohashi, T. Yagami, S. Tanaka, K. Ueda, Y. Sugiura, *J. Biol. Chem.* **2001**, *276*, 5836–5840.
[3] a) S. Futaki, W. Ohashi, T. Suzuki, M. Niwa, S. Tanaka, K. Ueda, H. Harashima, Y. Sugiura, *Bioconjugate Chem.* **2001**, *12*, 1005–1011; b) J. Fernandez-Carneado, M. J. Kogan, N. Van Mau, S. Pujals, C. Lopez-Iglesias, F. Heitz, E. Giralt, *J. Pept. Res.* **2005**, *65*, 580–590.
[4] a) J. Oehlke, A. Scheller, B. Wiesner, E. Krause, M. Beyermann, E. Klauschenz, M. Melzig, M. Bienert, *Biochim. Biophys. Acta Biomembr.* **1998**, *1414*, 127–139; b) J. Fernández-Carneado, M. J. Kogan, S. Pujals, E. Giralt, *Biopolymers* **2004**, *76*, 196–203; c) S. Pujals, J. Fernández-Carneado, C. Lopez-Iglesias, M. J. Kogan, E. Giralt, *Biochim. Biophys. Acta Biomembr.* **2006**, *1758*, 264–279.
[5] B. Gupta, T. S. Levchenko, V. P. Torchilin, *Adv. Drug Delivery Rev.* **2005**, *57*, 637–651.
[6] a) M. Bruchez, Jr., M. Moronne, P. Gin, S. Weiss, A. P. Alivisatos, *Science* **1998**, *281*, 2013–2016; b) S. G. Penn, L. He, M. J. Natan, *Curr. Opin. Chem. Biol.* **2003**, *7*, 609–615.
[7] D. Pantarotto, C. D. Partidos, J. Hoebeke, F. Brown, E. Kramer, J.-P. Briand, S. Muller, M. Prato, A. Bianco, *Chem. Biol.* **2003**, *10*, 961–966.
[8] a) A. de La Isla, W. Brostow, B. Bujard, M. Estevez, J. R. Rodriguez, S. Vargas, V. M. Castaño, *Mater. Res. Innovations* **2003**, *7*, 110–114; b) J. Ma, W. Huifen, L. B. Kong, K. W. Peng, *Nanotechnology* **2003**, *14*, 619.
[9] M. Shinkai, M. Yanase, M. Suzuki, H. Honda, T. Wakabayashi, J. Yoshida, T. Kobayashi, *J. Magn. Magn. Mater.* **1999**, *194*, 176–184.
[10] F. Marcucci, F. Lefoulon, *Drug Discovery Today* **2004**, *9*, 219–228.
[11] R. Weissleder, G. Elizondo, J. Wittenberg, C. A. Rabito, H. H. Bengele, L. Josephson, *Radiology* **1990**, *175*, 489–493.
[12] P. Alivisatos, *Nat. Biotechnol.* **2004**, *22*, 47–52.
[13] A. K. Iyer, G. Khaled, J. Fang, H. Maeda, *Drug Discovery Today* **2006**, *11*, 812–818.
[14] S. Li, L. Huan, *Mol. Pharm.* **2008**, *5*, 496–504.
[15] a) A. G. Tkachenko, H. Xie, D. Coleman, W. Glomm, J. Ryan, M. F. Anderson, S. Franzen, D. L. Feldheim, *J. Am. Chem. Soc.* **2003**, *125*, 4700–4701; b) A. G. Tkachenko, H. Xie, Y. Liu, D. Coleman, J. Ryan, W. R. Glomm, M. K. Shipton, S. Franzen, D. L. Feldheim, *Bioconjugate Chem.* **2004**, *15*, 482–490; c) J. de la Fuente, C. C. Berry, *Bioconjugate Chem.* **2005**, *16*, 1176–1180; d) A. M. Koch, F. Reynolds, M. F. Kircher, H. P. Merkle, R. Weissleder, L. Josephson, *Bioconjugate Chem.* **2003**, *14*, 1115–1121.
[16] S. Pujals, E. Giralt, *Adv. Drug Delivery Rev.* **2008**, *60*, 473–484.
[17] S. Pujals, E. Sabidó, T. Tarragó, E. Giralt, *Biochem. Soc. Trans.* **2007**, *35*, 794–796.
[18] J. Fernández-Carneado, M. J. Kogan, S. Castel, E. Giralt, *Angew. Chem.* **2004**, *116*, 1847–1850; *Angew. Chem. Int. Ed.* **2004**, *43*, 1811–1814.
[19] M. C. Daniel, D. Astruc, *Chem. Rev.* **2004**, *104*, 293–346.
[20] a) A. P. Alivisatos, *Sci. Am.* **2001**, *285*, 66–73; b) C. M. Niemeyer, *Angew. Chem.* **2001**, *113*, 4254–4287; *Angew. Chem. Int. Ed.* **2001**, *40*, 4128–4158.
[21] K. Hamad-Schifferli, J. J. Schwartz, A. T. Santos, S. G. Zhang, J. M. Jacobson, *Nature* **2002**, *415*, 152–155.
[22] M. J. Kogan, N. G. Bastus, R. Amigo, D. Grillo-Bosch, E. Araya, A. Turiel, A. Labarta, E. Giralt, V. F. Puntes, *Nano Lett.* **2006**, *6*, 110–115.
[23] I. H. El-Sayed, X. Huang, M. A. El-Sayed, *Nano Lett.* **2005**, *5*, 829–834.
[24] I. Brigger, C. Dubernet, P. Couvreur, *Adv. Drug Delivery Rev.* **2002**, *54*, 631–651.
[25] N. G. Bastús, E. Sánchez-Tilló, S. Pujals, C. Farrera, M. J. Kogan, E. Giralt, A. Celada, J. Lloberas, V. Puntes, *Mol. Immunol.* **2009**, *46*, 743–748.

 © 2009 Wiley-VCH Verlag GmbH & Co. KGaA, Weinheim

[26] a) H. Basch, M. A. Ratner, *J. Chem. Phys.* **2004**, *120*, 5771–5780; b) R. Lévy, N. T. K. Thanh, R. C. Doty, I. Hussain, R. J. Nichols, D. J. Schiffrin, M. Brust, D. G. Fernig, *J. Am. Chem. Soc.* **2004**, *126*, 10076–10084.
[27] a) J. Turkevich, P. C. Stevenson, J. Hillier, *Discuss. Faraday Soc.* **1951**, *11*, 55–75; b) J. Turkevich, P. C. Stevenson, J. Hillier, *J. Phys. Chem.* **1953**, *57*, 670–673; c) J. Turkevich, G. Garton, P. C. Stevenson, *J. Colloid Sci.* **1954**, *9*, 26–35; d) G. Frens, *Nat. Phys. Sci.* **1973**, *241*, 20–22; e) J. Kimling, M. Maier, B. Okenve, V. Kotaidis, H. Ballot, A. Plech, *J. Phys. Chem. B* **2006**, *110*, 15700–15707.
[28] M. G. Bellino, E. J. Calvo, G. Gordillo, *Phys. Chem. Chem. Phys.* **2004**, *6*, 424–428.
[29] J. D. Zhang, Q. J. Chi, J. U. Nielsen, E. P. Friis, J. E. T. Andersen, J. Ulstrup, *Langmuir* **2000**, *16*, 7229–7237.
[30] J. J. Storhoff, A. A. Lazarides, R. C. Mucic, C. A. Mirkin, R. L. Letsinger, G. C. Schatz, *J. Am. Chem. Soc.* **2000**, *122*, 4640–4650.
[31] C. A. Mirkin, *Inorg. Chem.* **2000**, *39*, 2258–2272.
[32] U. Kreibig, L. Genzel, *Surf. Sci.* **1985**, *156*, 678–700.
[33] K. Wojczykowski, D. Meissner, P. Jutzi, I. Ennen, A. Hütten, M. Fricke, D. Volkmer, *Chem. Commun.* **2006**, 3693–3695.
[34] M.-C. Bourg, A. Badia, R. B. Lennox, *J. Phys. Chem. B* **2000**, *104*, 6562–6567.
[35] F. Gisou van der Goot, J. Gruenberg, *Trends Cell Biol.* **2006**, *16*, 514–521.
[36] J. C. Kah, M. C. Olivo, C. G. Lee, C. J. Sheppard, *Mol. Cell. Probes* **2008**, *22*, 14–23.
[37] M. R. Howells, T. Breetz, H. N. Chapman, C. Cui, J. M. Holton, C. Jacobsen, J. Kirtz, E. Lima, S. Marchesini, H. Miao, D. A. Shapiro, J. C. H. Spencer, D. Starodub, *J. Electron Spectrosc. Relat. Phenom.* **2009**; DOI: 10.1016/j.elspec.2008.10.008.
[38] a) G. Schneider, *Ultramicroscopy* **1998**, *75*, 85–104; b) C. A. Larabell, M. A. Le Gros, *Mol. Biol. Cell* **2004**, *15*, 957–962; c) M. A. Le Gros, G. McDermott, C. A. Larabell, *Curr. Opin. Struct. Biol.* **2005**, *15*, 593–600.
[39] a) P. Guttmann, B. Niemann, S. Rehbein, C. Knöchel, D. Rudolph, G. Schmahl, *J. Phys. IV* **2003**, *13*, 85–90; b) G. Schneider, S. Heim, P. Guttmann, S. Rehbein, B. Neimann, *Proc. 8th Int. Conf. X-ray Microscopy, IPAP Conf. Series* **2006**, *7*, 349–352.
[40] a) E. E. Connor, J. Mwamuka, A. Gole, C. J. Murphy, M. D. Wyatt, *Small* **2005**, *1*, 325–327; b) N. G. Bastus, E. Casals, S. Vazquez-Campos, V. Puntes, *Nanotoxicology* **2008**, *2*, 99–112; c) E. Casals, S. Vázquez-Campos, N. G. Bastús, V. Puntes, *TrAC Trends Anal. Chem.* **2008**, *27*, 672–683.

Received: December 23, 2008
Published online on March 25, 2009

 © 2009 Wiley-VCH Verlag GmbH & Co. KGaA, Weinheim